

Perceptual Deep Neural Networks: Adversarial Robustness through Input Recreation

Danilo Vasconcellos Vargas
Kyushu University, Japan
vargas@inf.kyushu-u.ac.jp

Bingli Liao
Kyushu University, Japan

Takahiro Kanzaki
Kyushu University, Japan

Abstract

Adversarial examples have shown that albeit highly accurate, models learned by machines, differently from humans, have many weaknesses. However, humans' perception is also fundamentally different from machines, because we do not see the signals which arrive at the retina but a rather complex recreation of them. In this paper, we explore how machines could recreate the input as well as investigate the benefits of such an augmented perception. In this regard, we propose Perceptual Deep Neural Networks (φ DNN) which also recreate their own input before further processing. The concept is formalized mathematically and two variations of it are developed (one based on inpainting the whole image and the other based on a noisy resized super resolution recreation). Experiments reveal that φ DNNs and their adversarial training variations can increase the robustness substantially, surpassing both state-of-the-art defenses and pre-processing types of defenses in 100% of the tests. φ DNNs are shown to scale well to bigger image sizes, keeping a similar high accuracy throughout; while the state-of-the-art worsen up to 35%. Moreover, the recreation process intentionally corrupts the input image. Interestingly, we show by ablation tests that corrupting the input is, although counter-intuitive, beneficial. Thus, φ DNNs reveal that input recreation has strong benefits for artificial neural networks similar to biological ones, shedding light into the importance of purposely corrupting the input as well as pioneering an area of perception models based on GANs and autoencoders for robust recognition in artificial intelligence.

1. Introduction

Recent work has revealed that albeit highly accurate, deep neural networks are far from robust [36]. The lack of robustness exist even for extremely small perturbations and simple transformations [23, 10, 35]. A wide range of defenses were proposed in recent years [12, 13, 21, 25, 22]. However, most of them have shortcomings such as relying on obfuscated

gradients [1] or being biased by the type of perturbation used to train (e.g., adversarial training) [19, 17].

Humans are less affected by small changes in the input. Interestingly, this is true even when part of the input is completely removed; which happens every second. Each of our eyes have a blind spot¹ where light cannot be perceived. Albeit this limitation, when we close one eye we do not see a black spot but a completely filled perception of an image [7, 18]. This is an example of how the brain is always predicting what it is viewing, revealing that biological perceptual systems are active rather than passive [24]. Thus, the images we see every second is rather a creation than mere signals that arrived in the brain, also called perception filling-in and related to predictive coding [5, 30, 9]. In this context, we raise the following question:

*Could deep neural networks also benefit
from actively creating its own input?*

To answer the question above we developed two perceptual systems that recreate the input image with predictions of it. One is based on inpainting all parts of the image while the other is based on recreating a super resolution of the image and then resizing it (Section 3.2). The recreated input is then fed to a deep neural network which has no access to the original input (Figure 1). Attacks on both systems suggest that by recreating the input, robustness against adversarial attacks increase. Furthermore, the input recreation is not mutually exclusive with many of the previous defenses. It can be used together with adversarial training, for example, to improve further robustness.

Our contributions. In this paper, we present input recreation as a novel paradigm to enhance robustness against adversarial samples. The key contributions can be summarized as follows:

- We introduce deep neural networks (DNN) that recreate their own input based solely on contextual hints,

¹The blind spot in each eye is where the optic nerve passes through the optic disc and therefore no photoreceptor cells are present.

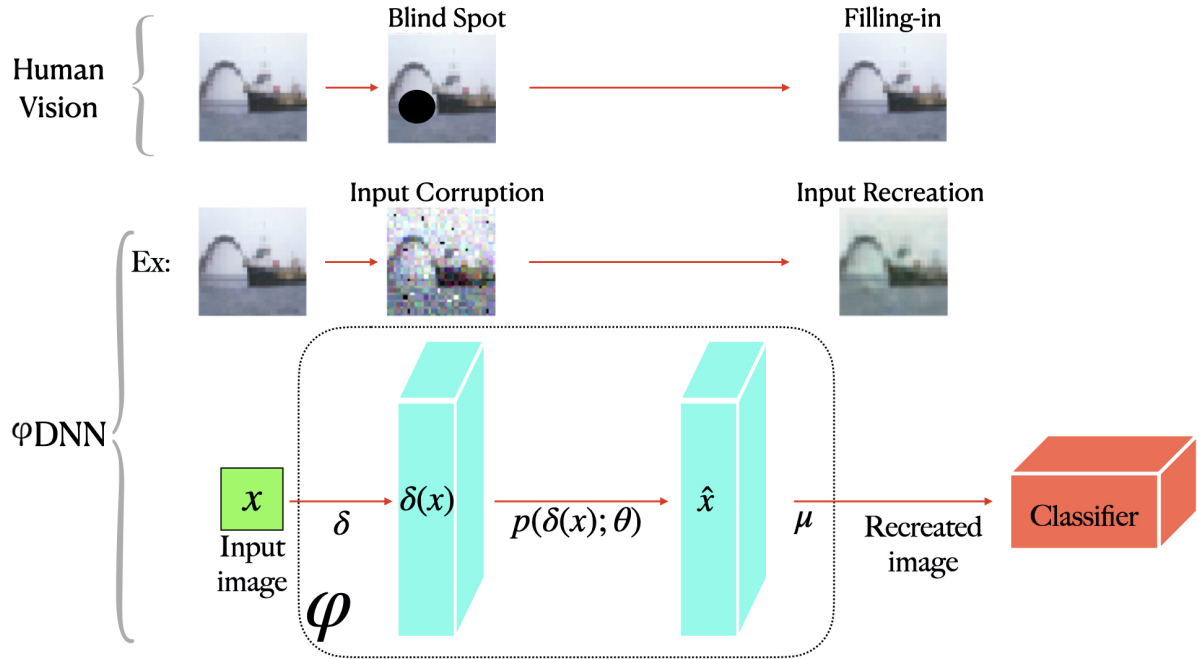


Figure 1: Illustration of the proposed φ DNN architecture and its similarity to the filling-in phenomena in human vision. Input x is initially corrupted by $\delta(x)$, removing some information while keeping contextual clues. $p(\delta(x); \theta)$ uses this corrupted image to predict a partial (or whole) recreation which is then aggregated with function μ to compose a complete recreated image. This recreated image is sent to the vanilla classifier.

called perceptual DNNs (φ DNN). We describe φ DNNs formally and conduct experiments on two different implementations of it.

- We propose an inpainting based φ DNN. It works by predicting removed parts of the image and then joining the predicted parts together into a single completely recreated image. This recreated image is then used as input to a DNN.
- We propose a super resolution based φ DNN which recreates a higher resolution version of the input excluding at the same time any noise present in the original one. The image is later resized and inputted to a DNN.
- The results suggest that approaches with active perceptual systems recreating their own input can achieve higher robustness than their counterparts. This is true not only for the best performing system but most of its numerous variations, revealing a strength of the approach. Moreover, φ DNNs can be used jointly with other defenses to increase robustness further.
- Experiments reveal that, for neural networks able to recreate their own input, always purposely corrupting the input (for both training and testing) is mostly beneficial.

2. Related Works

Attack Methods. In this paper, we make use of attack methods for the sole purpose of evaluating the robustness of defenses and neural network models. Several attack models have been proposed in recent studies. They can be broadly categorized into white box [36, 12, 23, 3] and black box attacks [26, 2, 16, 38, 8]. Many white box models can be summarized as follows. Given a target classifier C and an input pair (x, y) . Let \mathcal{L} be the adversarial loss for the classifier $C(x')$ e.g., the cross-entropy loss, and the ℓ_p norm used to measure the distance between the legitimate input x and the adversarial input x' . Generally, white box attack methods have been proposed by solving the constrained optimization problem:

$$\min_{x'} \mathcal{L}(C(x'), y), \quad \text{s.t.} \quad \|x - x'\|_p \leq \epsilon. \quad (1)$$

Examples of white box attacks are FGSM [12], one of the earliest white box attacks, which uses one-step approach to determine the direction to change the pixel value, and an improved method called projected gradient descent (PGD) with a multiple-step variant [23]. In contrast, black box attacks have been proposed under more critical and practical conditions with the trade-off of being slower. Here, we are also interested in black box attacks which are not based on estimating gradients and therefore can find adversarial

samples even when the gradient is masked [1]. Therefore, tests with more straightforward black box attack methods based on evolutionary strategy such as the one-pixel attack and few-pixel attack fits the purpose [35].

Defenses to Adversarial Attacks. Recent studies have proposed various defense mechanisms against the threat of adversarial attacks. Albeit recent efforts, there is not yet a completely effective method. Defensive distillation, for example, proposed a smaller neural network which squeezed the content learned by the original one [27], however, it was shown to lack robustness in a later paper [3]. Adversarial training which was firstly proposed by Goodfellow *et al.* [12] increases the robustness by adding adversarial examples to the training set [15], [23]. Similarly, adversarial training was also shown vulnerable to attacks in [37]. Other defenses include pre-processing defenses such as the feature squeezing (FS) and spatial smoothing (SS) [42]. The objective here is to remove adversarial perturbation in a pre-processing stage. Recently there are a huge number of defenses proposed, however, they use mostly variations of gradient masking to avoid being attacked which do not confer greater security [1]. Regarding GAN based defenses, Defense-GAN [32] is based on training a generative adversarial network (GAN) to learn the distribution of original images. Each input would then be used to search for the closest projected input image learned by the generator before proceeding to classification. One of the main shortcomings is that the distribution learned by the generator is strictly limited by the training data set and the input image might be mapped into an illegitimate space. Albeit using GANs in our proposed approach, it shares no other similarities to Defense-GAN. Here, GANs predict parts of the input using the contextual information present, and only after the input has been purposely corrupted.

Predictive Coding. Although φ DNNs do not necessarily use many of the components of predictive coding, it is loosely based on it. Predictive coding is a theory in neuroscience which postulates that the brain achieves high visual robustness by dynamically updating and predicting neural activities from the environment [28]. Previous studies have shown that the brain uses similar representations to CNNs, but CNNs are not as robust as the brain [4, 41]. Though there is still no perfect theoretical explanation for how it works, biological plausible models describe it as a recurrently connected hierarchical neural networks [34]. Recent research on predictive coding based CNNs imitating the feedforward, feedback, and recurrent connections performed well in object recognition tasks [40].

This work makes use of both Generative Adversarial Network (GAN) and AutoEncoder (AE) to recreate the images. They are described briefly as follows.

2.1. Generative Adversarial Network

Generative Adversarial Network (GAN) is a powerful generative model that consists of two neural networks: a generator network which learns the probability distribution of the input and a discriminator network which distinguishes between generated data and the input data [11].

Super-resolution GAN (SRGAN). Super-resolution GAN (SRGAN) generates a photo-realistic high-resolution (HR) image from its downsampled low-resolution (LR) input image. In [20], they used VGG-19 network to extract high dimension features and designed an alternative function, the perceptual loss function, which consists of content loss and adversarial loss to solve the following min-max optimization problem:

$$\min_G \max_D \mathbb{E}_{I^{HR} \sim p_{train}(I^{HR})} [\log D(I^{HR})] + \mathbb{E}_{I^{LR} \sim P_G(I^{LR})} [\log(1 - D(G(I^{LR})))] \quad (2)$$

Here, the generative model G maps a given LR input I^{LR} to its HR counterpart I^{HR} . The discriminator D is trained to distinguish between the produced I^{HR} images from real inputs.

2.2. Autoencoder based Inpainting

Inpainting is defined as the synthesis of content to fill missing image parts. Here, we use an AE to predict the missing pixels with a simple UNET-like architecture [39, 31]. Let a masked image x_0 be represented as $x_0 = x \odot (1 - M)$, in which M is a binary mask, x is the original input image and \odot is the element-wise product operation. Inpainting can be formulated as the following energy minimization problem:

$$\min_{\theta} E(F(x_0; \theta); x),$$

$$E(F(x_0; \theta); x) = |(F(x_0; \theta) - x)|,$$

where F is the resulting function from the AE with parameters θ .

3. φ DNNs

In this section, we describe formally the φ DNN architecture, its motivation as well as two different implementations of it.

3.1. Technical Motivation Behind Input Recreation

Beyond the bio-inspired aspect, there are some technical importance for recreating the input in a similar way to humans and other animals. First, by recreating the input, the neural network and not the environment defines which input will be responsible for the output of the system. This type

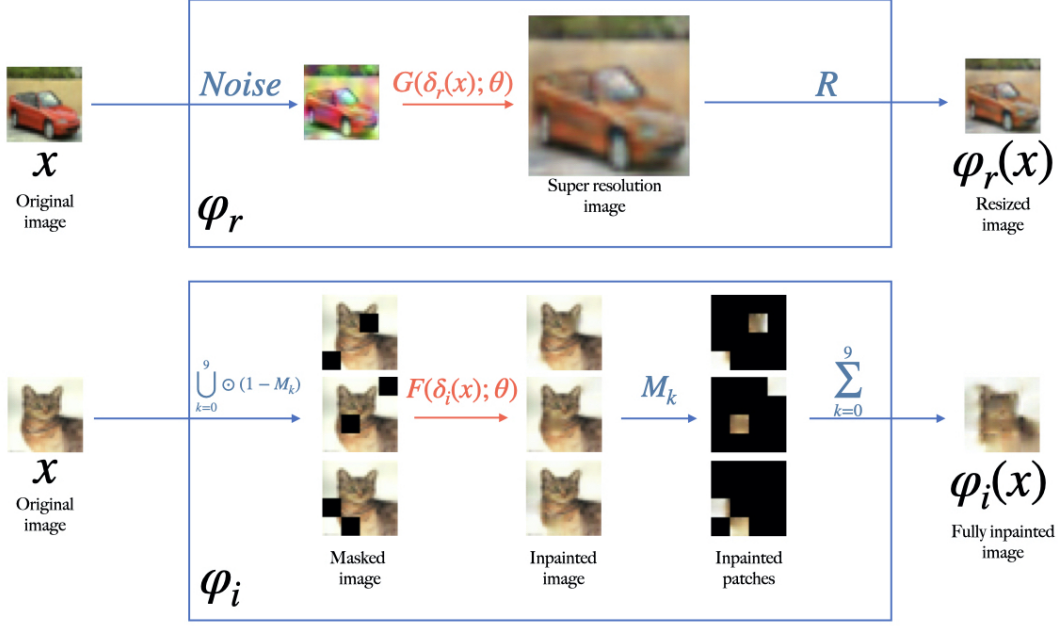


Figure 2: Illustration of the two implementations of φ DNNs proposed: Noisy Super-resolution Recreation (top) and Full Inpainting Recreation (bottom).

of actively modified input provides further control of the input to avoid contextual problems or other issues beyond adversarial samples. Second, it is now possible to constrain the probability distribution of the input further. This can be done in many ways and is only slightly explored here with added noise. Third, with perceptual changes happening all the time, attacking becomes a time-varying function which might be impossible to repeat. This would make calculated attacks near impossible. Fourth, when facing φ DNNs, the attacker has less information about the network for he/she does not know even the input now. Lastly, gradient-based and gradient estimation based approaches tend to perform poorly if the input is changed substantially by the recreation process.

3.2. φ DNN's Architecture

Consider the perceptual tuple φ and its respective function $\varphi(x)$ as follows:

$$\varphi := \langle \delta, p(\delta(x); \theta), \mu \rangle, \quad (3)$$

$$\varphi(x) = \mu(p(\delta(x); \theta)), \quad (4)$$

where δ is a function that corrupts the input, removing some information from it and returning one or multiple corrupted images; $p(\delta(x); \theta)$ is the probability distribution learned by a model that predicts x from the corrupted input $\delta(x)$ based on its learned weights θ ; and μ is the aggregation function which joins partial recreations (when present) into a single recreated image.

φ DNN is defined as follows:

$$\varphi\text{DNN} := C(\varphi(x)), \quad (5)$$

in which C is a classifier that receives as input the output from the perceptual function $\varphi(x)$.

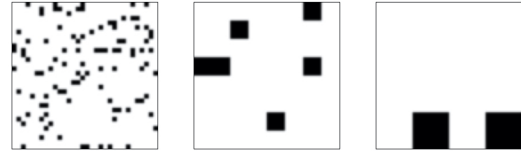


Figure 3: Three masks created for FIR with grid size of respectively (from left to right) 1, 4 and 8.

Noisy Super-Resolution Recreation (NSR) Here we define an implementation of the φ DNN's architecture using super resolution and images corrupted with noise. Note that images are always corrupted with noise (i.e., in both training and testing). Let x be a given input and R a function which resizes the high resolution image to the original resolution. The process can be defined as follows:

$$\varphi_r := \langle \delta_r, p_r(\delta(x); \theta_r), \mu_r \rangle, \quad (6)$$

$$\text{where } \delta_r = \text{Noise}, p_r = G(\delta(x); \theta), \mu_r = R.$$

note that Noise is an arbitrary noise function which returns a noisy image. $G(\delta(x); \theta)$ is the generator of SRGAN which

Table 1: Comparison between Feature Scattering (the current state-of-the-art defense) and the two proposed φ DNNs with a simple adversarial training (NSR_{adv} and FIR_{adv}) on CIFAR10, SVHN and Imagenette. Results show the accuracy of defenses under attack. For reference, we include the φ DNNs without adversarial training (NSR and FIR), only ResNet with the same simple adversarial training used on NSR_{adv} and FIR_{adv} (ResNet_{adv}); as well as vanilla ResNet. ResNet_{pruned} means the trained ResNet is pruned 50%, retrained and then ultimately pruned to 80%.

Defense	test acc	1px attack	10px attack	FGSM ($\epsilon = 8$)	PGD ($\epsilon = 8$)
Imagenette					
Ours: NSR_{adv}	77.0	75.3	75.6	51.6	46.7
Ours: FIR_{adv}	78.1	73.7	62.9	74.8	66.2
FScattering	72.4	59.5	52.2	42.3	43.2
NSR	81.7	77.5	77.6	37.4	45.8
FIR	85.4	81.1	76.9	5.0	0.3
CIFAR10					
Ours: NSR_{adv}	82.7	78.1	73.9	75.3	75.5
Ours: FIR_{adv}	88.5	73.6	50.4	88.3	82.5
FScattering	90.0	72.2	47.7	78.4	70.5
TRADES	87.4	—	—	—	51.6
LLR	86.8	—	—	—	54.2
NSR	83.8	78.3	73.9	63.4	69.3
FIR	89.4	78.1	54.2	25.6	5.0
ResNet _{adv}	89.2	60.3	17.8	25.2	0.0
ResNet	93.0	62.1	18.2	17.7	0.0
ResNet _{pruned}	85.8	41.9	4.1	63.8	56.8
SVHN					
Ours: NSR_{adv}	92.4	89.1	87.7	85.0	86.9
Ours: FIR_{adv}	93.0	80.9	53.9	93.0	91.5
FScattering	96.2	81.4	46.0	83.5	52.0
NSR	93.0	90.2	90.1	74.4	85.6
FIR	96.4	80.4	57.1	49.0	7.9

maps an image from low resolution to high resolution and tries to clean the always present noise (illustrated in Figure 2).

Full Inpainting Recreation (FIR) To demonstrate that φ DNNs can be developed in many forms, here, we propose a φ DNN based on inpainting the whole image. Specifically, φ_i is defined as follows.

$$\varphi_i := \langle \delta_i, p_i(\delta(x); \theta_i), \mu_i \rangle, \quad (7)$$

$$\text{where } \delta_i(x) = \bigcup_{k=0}^9 \odot(1 - M_k) \cdot x,$$

$$p_i = F(\delta(x); \theta), \mu_i(x) = \sum_{k=0}^9 M_k \cdot x,$$

where M_k are masks such that their sum is equal to the identity matrix ($\sum_{k=0}^9 M_k = I$) and their multiplication is equal to 0 ($\prod_{k=0}^9 M_k = 0$). Therefore, each of the masks

hide a specific part of the image; and together they mask the whole image. $\delta_i(x)$ (i.e., $\bigcup_{k=0}^9 \odot(1 - M_k) \cdot x$) creates a set with 10 masked inputs. All masked inputs are then inpainted with $F(\delta(x); \theta)$ and lastly all inpainted parts are joined together through $\sum_{k=0}^9 M_k \cdot x$. Figure 2 shows an illustration of the process.

4. Experiments

To evaluate φ DNN architecture, we test here the robustness of two implementations of it (i.e., FIR and NSR) by attacking them with different types of attacks. The proposed architecture is also compared with other defenses in three datasets (CIFAR, SVHN and a subset of Imagenet called Imagenette [33]).

To evaluate the robustness of systems avoiding biases and the sole presence of gradient masking, we employ two white box attacks (FGSM and PGD) as well as non-gradient based black box attacks (one pixel and ten pixel attack). In this

Table 2: Comparison of proposed methods with other pre-processing based defenses. NSR and FIR models use the best setting from Tables 3 and 4 while the other ones use AllConv and the best settings out of a couple of experiments.

Defense	test acc	1px attack	10px attack	FGSM ($\epsilon = 8$)	PGD ($\epsilon = 8$)
Ours: NSR	83.8	78.3	73.9	63.4	69.3
Ours: FIR	89.4	73.2	54.2	25.6	5.0
FS	79.2	42.7	10.5	17.3	0.0
SS	78.6	69.6	38.8	20.1	0.9
JPEG	73.0	21.0	1.5	31.5	5.4
LS	91.4	48.6	15.0	50.5	0.0

paper, every attack is repeated for 500 uniformly sampled random images of the test data set with the average attack accuracy being reported. For all experiments, the CIFAR-10 dataset is normalized to the range $[0, 1]$. The machines used in the experiments are equipped with NVIDIA GeForce RTX 2080 Ti and AMD Ryzen 9 3950x 16-core.

Regarding FIR, 10 masks are created, each of them removing 10% of the image. (Figure 3). To create the masks, a grid of a given size is set over the 32×32 image and then multiple pieces of this grid are randomly selected to form one mask. Pieces are selected until 10% of the image is covered. The inpainting model is trained with a corresponding mask size covering 10% of the image and with epochs and batch size of respectively 20 and 32.

Regarding NSR, to create the training dataset for SRGAN we resize CIFAR-10 dataset to 128×128 as the high resolution ground truth and add noise to the training dataset during training. The type of noise used is bi-linear interpolation for both up and downsizing. In order to match with the normalization, we replace tanh with sigmoid as the activation function for the last convolution layer in SRGAN’s generator. We train SRGAN with 1000 epochs and set batch size to 20 to ensure convergence.

4.1. Comparison with other Defenses

Table 1 compares the last development in adversarial training, i.e. Feature Scattering [43], with the proposed algorithms and variations of them trained with a simple adversarial training. Other state-of-the-art defenses such as LLR and TRADES are also included in some of tests, using the original results reported from their papers [29, 44].

Results show that both φ DNNs with adversarial training surpass FScattering for all of the attacks (the only exception is the SVHN test in which FIR_{adv} gets 80.9% against 81.4% achieved by FScattering). It is known that adversarial training methods such as FScattering perform poorly when the attacking distribution differ from the data used to learn. This applies to FScattering as well which can be attacked with more than 50% attack accuracy with 10px attack. Having said that, it is impressive that both NSR and FIR can surpass

FScattering even on FGSM and PGD which are close to the augmented distribution of noisy images FScattering used to learn. Notice that the same adversarial training that has little change on the vanilla Resnet (i.e., $ResNet_{adv}$) is very effective on NSR and FIR. For example, in CIFAR under a PGD attack, FIR_{adv} is 82.5% accurate against a 5% accuracy of the vanilla FIR and a 0% accuracy of the same adversarial training applied on a vanilla ResNet. Thus, it is expected that if a state-of-the-art adversarial training is applied to NSR and FIR, their robustness should improve even further. Pruned networks were also added to demonstrate that lower accuracy pruned neural networks are not comparable with current defenses.

In fact, if we take into account that FScattering and φ DNN are (a) different in nature and (b) can be also used together. It can be justified that φ DNNs should be compared with other pre-processing defenses and not adversarial training ones. We follow this rational and compare the proposed methodology in Table 2 with other pre-processing defenses such as FS, SS, JPEG compression defence (JPEG) [6] and Label Smoothing (LS) [14]. All defenses used ResNet with the same type of augmentation. Note that we also tried to include DefenseGAN but it failed to learn properly on CIFAR10.

Both φ DNNs surpass all others in most of the attacks. The result is expected since φ DNNs do not only pre-process images, they recreate them based on contextual information and previous learned distribution. The only exception is FIR for FGSM and PGD (Table 2). FIR’s poor results on PGD and FGSM are less obvious. It is related to the grid size which is discussed in Section 4.3.

4.2. NSR Analysis: When Losing Information is Beneficial

NSR corrupts the input image possibly losing some information. Here we will investigate if this loss of information has any deleterious consequences. We will also analyze the behavior of NSR on adversarial samples. To analyze the influence of the initial input corruption by $\delta_r(x)$, an ablation test is made, in which $\delta_r(x)$ is removed from $\varphi_r(x)$ (this

Table 3: Attack accuracy for both NSR and SR (NSR without the added noise $\delta_r(\cdot)$) trained with different types of noise and connected to ResNet. We tested Gaussian noise with 0 mean (μ), and variances (σ^2) of 0.01. For Panda noise, the scalar number (0.01) represents the probability (α and β) of white and black pixels present in the image. $A + B$ represents that two types of noises A and B are summed together. The subscript T means that the classifier was retrained with a data set made of recreated images (i.e., images from $\varphi_r(x)$).

Defense	Noise	test acc	10px attack	FGSM ($\epsilon = 8$)	PGD ($\epsilon = 8$)
NSR	+ResNet[Guassian0.01]	79.2	60.5	64.5	68.1
SR	+ResNet[Guassian0.01]	77.4	16.2	61.5	68.9
NSR	+ResNet[Panda0.01]	91.0	49.1	70.8	67.2
SR	+ResNet[Panda0.01]	91.5	30.8	25.3	11.0
NSR	+ResNet[Guassian+Panda]	77.0	64.5	62.8	66.7
SR	+ResNet[Guassian+Panda]	81.9	37.9	61.4	70.6
NSR	+ResNet[Guassian+Panda] _T	83.8	74.6	63.4	69.3
SR	+ResNet[Guassian+Panda] _T	84.5	44.6	65.9	73.0

Table 4: Comparing the difference of grid size on FIR’s accuracy and robustness. ResNet is the vanilla classifier while FIR_1^+ , FIR_4^+ and FIR_8^+ means using ResNet in the FIR’s architecture with grid size of respectively 1, 4 and 8. Each inpainting model is trained with the corresponding grid size only, and the classifier model is trained with corresponding inpainting image from $\varphi_i(x)$.

	Test accuracy	1px attack	10px attack	FGSM ($\epsilon = 8$)	PGD ($\epsilon = 8$)
ResNet	93.0	56.0	18.2	17.7	0.0
FIR_1	89.4	73.2	54.2	25.6	5.0
FIR_4	82.7	69.2	43.2	48.0	49.1
FIR_8	73.5	59.0	25.9	49.5	53.7

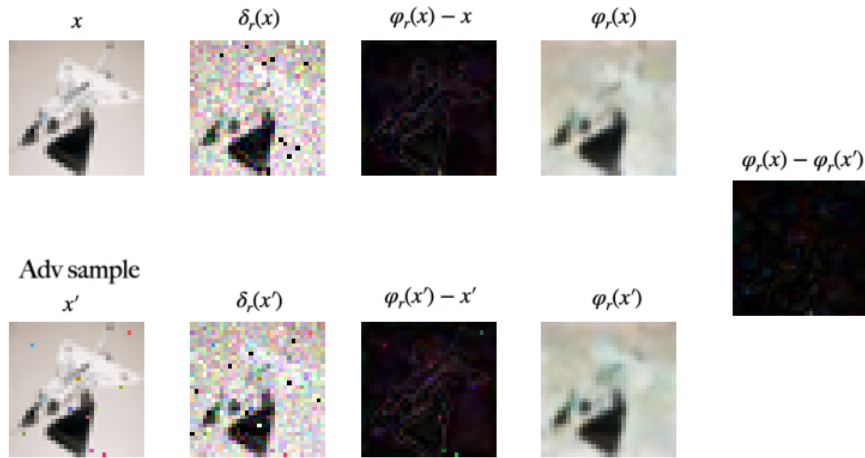


Figure 4: Behavior of an image sample x and its respective adversarial sample x' throughout $\varphi_r(x)$.

algorithm is called SR in Table 3). Results show an increased robustness and similar accuracy. Specifically, in 8 out of 12

tests, the robustness of NSR surpassed the ablated algorithm SR. Regarding the accuracy, both NSR and SR performed

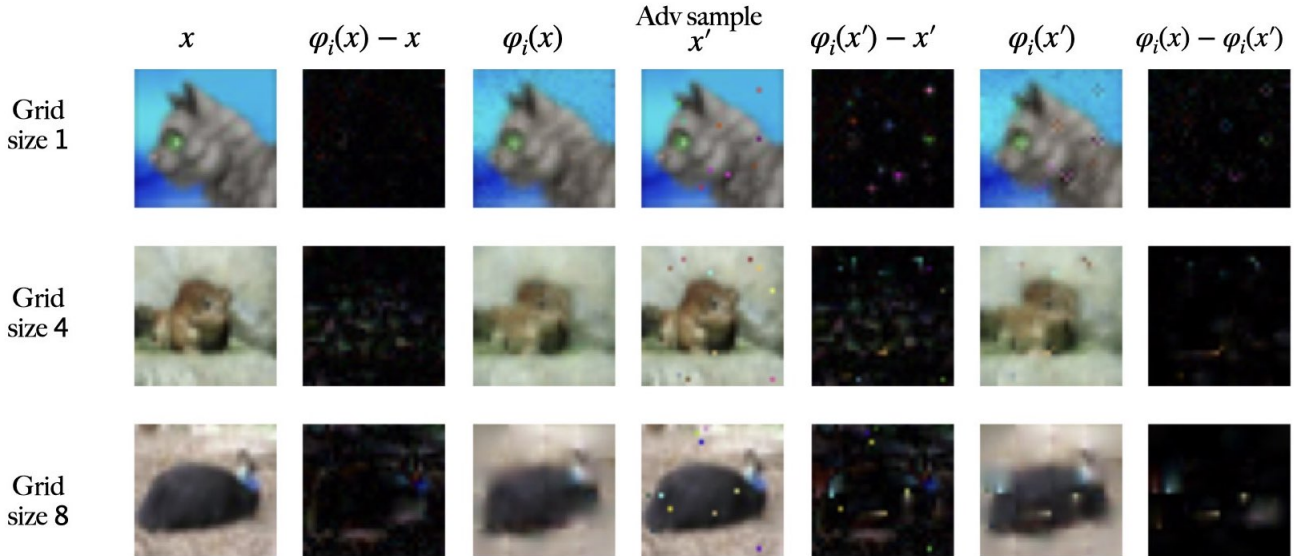


Figure 5: Behavior of $\varphi_i(x)$ on an image sample x and its respective adversarial sample x' .

similarly.

These results reveal, perhaps counter-intuitively, that always adding noise ($\delta_r(x)$) to the input is mostly beneficial for neural networks that recreate their input. On average, it usually improves robustness while leaving accuracy unchanged. There are two reasons for such a behavior: (a) always adding noise constrains the image distribution to non-smooth pixel transitions and (b) an always changing input is harder to attack.

4.3. FIR Analysis

In this section, FIR will be analyzed with relation to its grid size. For L0 attacks (1px, 5px and 10px attacks), FIR performs better with lower grid values while higher grid values are better suited to L ∞ attacks (PGD and FGSM) (Table 4). This is expected since L0 attacks perturbs fewer pixels and therefore punctual corrections are better. The opposite is true for L ∞ . Attacking FIR is difficult because for a pixel to be modified in the final image $\varphi_i(x)$, many pixels around it must be changed (for lower grid values) or pixels near the mask needs to be changed (for higher grid values). This creates a bigger burden on the attacker and causes many attacks to fail. A simple version of adversarial training (with FGSM created adversarial samples) improves substantially the advantages of FIR, allowing it to even surpass the state-of-the-art (Table 1).

5. Conclusions

In this paper, we proposed φ DNNs which make use of corrupting functions and context-based prediction to recreate

the input. We showed that, perhaps surprisingly, corrupting the input is beneficial to robustness. Moreover, two implementations of φ DNNs surpassed the state-of-the-art while possessing much better scaling for datasets with bigger image sizes. Note that the implementations used here do not utilize state-of-the-art GANs or AEs as well as only a classic adversarial training scheme. Therefore, state-of-the-art GANs/AEs/adversarial training should increase further the results reported here, which are already surpassing the state-of-the-art in all of the tests.

Thus, this paper proposes a novel paradigm for robust neural networks with state-of-the-art results which should, hopefully, incentive further investigation into φ DNNs and other perception models. It also opens new paths for robust artificial intelligence, towards safer applications.

References

- [1] Anish Athalye, Nicholas Carlini, and David Wagner. Obfuscated gradients give a false sense of security: Circumventing defenses to adversarial examples. In *Proceedings of the 35th International Conference on Machine Learning, ICML 2018*, July 2018.
- [2] W. Brendel, J. Rauber, and M. Bethge. Decision-based adversarial attacks: Reliable attacks against black-box machine learning models. In *International Conference on Learning Representations*, 2018.
- [3] Nicholas Carlini and David Wagner. Towards evaluating the robustness of neural networks. In *2017 IEEE*

- symposium on security and privacy (sp)*, pages 39–57. IEEE, 2017.
- [4] Radoslaw Martin Cichy, Aditya Khosla, Dimitrios Pantazis, Antonio Torralba, and Aude Oliva. Comparison of deep neural networks to spatio-temporal cortical dynamics of human visual object recognition reveals hierarchical correspondence. *Scientific reports*, 6:27755, 2016.
- [5] Andy Clark. Whatever next? predictive brains, situated agents, and the future of cognitive science. *Behavioral and brain sciences*, 36(3):181–204, 2013.
- [6] Nilaksh Das, Madhuri Shanbhogue, Shang-Tse Chen, Fred Hohman, Li Chen, Michael E Kounavis, and Duen Horng Chau. Keeping the bad guys out: Protecting and vaccinating deep learning with jpeg compression. *arXiv preprint arXiv:1705.02900*, 2017.
- [7] Peter De Weerd, Ricardo Gattass, Robert Desimone, and Leslie G Ungerleider. Responses of cells in monkey visual cortex during perceptual filling-in of an artificial scotoma. *Nature*, 377(6551):731–734, 1995.
- [8] Yinpeng Dong, Hang Su, Baoyuan Wu, Zhifeng Li, Wei Liu, Tong Zhang, and Jun Zhu. Efficient decision-based black-box adversarial attacks on face recognition. In *Proceedings of the IEEE Conference on Computer Vision and Pattern Recognition*, pages 7714–7722, 2019.
- [9] Benedikt V Ehinger, Katja Häusser, Jose P Ossandon, and Peter König. Humans treat unreliable filled-in percepts as more real than veridical ones. *Elife*, 6:e21761, 2017.
- [10] Logan Engstrom, Dimitris Tsipras, Ludwig Schmidt, and Aleksander Madry. A rotation and a translation suffice: Fooling cnns with simple transformations. *ArXiv*, abs/1712.02779, 2017.
- [11] Ian Goodfellow, Jean Pouget-Abadie, Mehdi Mirza, Bing Xu, David Warde-Farley, Sherjil Ozair, Aaron Courville, and Yoshua Bengio. Generative adversarial nets. In *Advances in neural information processing systems*, pages 2672–2680, 2014.
- [12] Ian Goodfellow, Jonathon Shlens, and Christian Szegedy. Explaining and harnessing adversarial examples. In *International Conference on Learning Representations*, 2015.
- [13] Kathrin Grosse, Praveen Manoharan, Nicolas Papernot, Michael Backes, and Patrick McDaniel. On the (statistical) detection of adversarial examples. *arXiv preprint arXiv:1702.06280*, 2017.
- [14] Tamir Hazan, George Papandreou, and Daniel Tarlow. *Perturbations, Optimization, and Statistics*. MIT Press, 2016.
- [15] Ruitong Huang, Bing Xu, Dale Schuurmans, and Csaba Szepesvári. Learning with a strong adversary. *arXiv preprint arXiv:1511.03034*, 2015.
- [16] Andrew Ilyas, Logan Engstrom, Anish Athalye, and Jessy Lin. Black-box adversarial attacks with limited queries and information. In *Proceedings of the 35th International Conference on Machine Learning, ICML 2018*, July 2018.
- [17] Harini Kannan, Alexey Kurakin, and Ian J. Goodfellow. Adversarial logit pairing. *ArXiv*, abs/1803.06373, 2018.
- [18] Hidehiko Komatsu. The neural mechanisms of perceptual filling-in. *Nature reviews neuroscience*, 7(3):220–231, 2006.
- [19] Alexey Kurakin, J. Ian Goodfellow, and Samy Bengio. Adversarial machine learning at scale. *international conference on learning representations*, 2017.
- [20] Christian Ledig, Lucas Theis, Ferenc Huszár, Jose Caballero, Andrew Cunningham, Alejandro Acosta, Andrew Aitken, Alykhan Tejani, Johannes Totz, Zehan Wang, et al. Photo-realistic single image super-resolution using a generative adversarial network. In *Proceedings of the IEEE conference on computer vision and pattern recognition*, pages 4681–4690, 2017.
- [21] Xin Li and Fuxin Li. Adversarial examples detection in deep networks with convolutional filter statistics. In *Proceedings of the IEEE International Conference on Computer Vision*, pages 5764–5772, 2017.
- [22] Xingjun Ma, Bo Li, Yisen Wang, Sarah M Erfani, Sudanthi Wijewickrema, Grant Schoenebeck, Dawn Song, Michael E Houle, and James Bailey. Characterizing adversarial subspaces using local intrinsic dimensionality. In *6th International Conference on Learning Representations, ICLR 2018*, 2018.
- [23] Aleksander Madry, Aleksandar Makelov, Ludwig Schmidt, Dimitris Tsipras, and Adrian Vladu. Towards deep learning models resistant to adversarial attacks. In *International Conference on Learning Representations*, 2018.
- [24] James L McClelland and David E Rumelhart. An interactive activation model of context effects in letter perception: I. an account of basic findings. *Psychological review*, 88(5):375, 1981.

- [25] Jan Hendrik Metzen, Tim Genewein, Volker Fischer, and Bastian Bischoff. On detecting adversarial perturbations. In *Proceedings of 5th International Conference on Learning Representations (ICLR)*, 2017.
- [26] Nicolas Papernot, Patrick McDaniel, Ian Goodfellow, Somesh Jha, Z Berkay Celik, and Ananthram Swami. Practical black-box attacks against machine learning. In *Proceedings of the 2017 ACM on Asia conference on computer and communications security*, pages 506–519, 2017.
- [27] Nicolas Papernot, Patrick McDaniel, Xi Wu, Somesh Jha, and Ananthram Swami. Distillation as a defense to adversarial perturbations against deep neural networks. In *2016 IEEE Symposium on Security and Privacy (SP)*, pages 582–597. IEEE, 2016.
- [28] Cyriel MA Pennartz. *The brain’s representational power: on consciousness and the integration of modalities*. MIT Press, 2015.
- [29] Chongli Qin, James Martens, Sven Gowal, Dilip Krishnan, Krishnamurthy Dvijotham, Alhussein Fawzi, Soham De, Robert Stanforth, and Pushmeet Kohli. Adversarial robustness through local linearization. In *Advances in Neural Information Processing Systems*, pages 13847–13856, 2019.
- [30] Rajesh PN Rao and Dana H Ballard. Predictive coding in the visual cortex: a functional interpretation of some extra-classical receptive-field effects. *Nature neuroscience*, 2(1):79–87, 1999.
- [31] Olaf Ronneberger, Philipp Fischer, and Thomas Brox. U-net: Convolutional networks for biomedical image segmentation. In *International Conference on Medical image computing and computer-assisted intervention*, pages 234–241. Springer, 2015.
- [32] Pouya Samangouei, Maya Kabkab, and Rama Chellappa. Defense-GAN: Protecting classifiers against adversarial attacks using generative models. In *International Conference on Learning Representations*, 2018.
- [33] Sam Shleifer and Eric Prokop. Using small proxy datasets to accelerate hyperparameter search. *arXiv preprint arXiv:1906.04887*, 2019.
- [34] Olaf Sporns and Jonathan D Zwi. The small world of the cerebral cortex. *Neuroinformatics*, 2(2):145–162, 2004.
- [35] Jiawei Su, Danilo Vasconcellos Vargas, and Kouichi Sakurai. One pixel attack for fooling deep neural networks. *IEEE Transactions on Evolutionary Computation*, 23(5):828–841, 2019.
- [36] Christian Szegedy, Wojciech Zaremba, Ilya Sutskever, Joan Bruna, Dumitru Erhan, Ian Goodfellow, and Rob Fergus. Intriguing properties of neural networks. In *International Conference on Learning Representations*, 2014.
- [37] Florian Tramèr, Alexey Kurakin, Nicolas Papernot, Ian Goodfellow, Dan Boneh, and Patrick Drew McDaniel. Ensemble adversarial training: Attacks and defenses. In *6th International Conference on Learning Representations, ICLR 2018*, 2018.
- [38] Chun-Chen Tu, Paishun Ting, Pin-Yu Chen, Sijia Liu, Huan Zhang, Jinfeng Yi, Cho-Jui Hsieh, and Shin-Ming Cheng. Autozoom: Autoencoder-based zeroth order optimization method for attacking black-box neural networks. In *Proceedings of the AAAI Conference on Artificial Intelligence*, volume 33, pages 742–749, 2019.
- [39] Dmitry Ulyanov, Andrea Vedaldi, and Victor Lempitsky. Deep image prior. In *Proceedings of the IEEE Conference on Computer Vision and Pattern Recognition*, pages 9446–9454, 2018.
- [40] Haiguang Wen, Kuan Han, Junxing Shi, Yizhen Zhang, Eugenio Culurciello, and Zhongming Liu. Deep predictive coding network for object recognition. In Jennifer Dy and Andreas Krause, editors, *Proceedings of the 35th International Conference on Machine Learning*, volume 80 of *Proceedings of Machine Learning Research*, pages 5266–5275, Stockholm, Stockholm, 10–15 Jul 2018. PMLR.
- [41] Haiguang Wen, Junxing Shi, Yizhen Zhang, Kun-Han Lu, Jiayue Cao, and Zhongming Liu. Neural encoding and decoding with deep learning for dynamic natural vision. *Cerebral Cortex*, 28(12):4136–4160, 2018.
- [42] Weilin Xu, David Evans, and Yanjun Qi. Feature squeezing: Detecting adversarial examples in deep neural networks. *arXiv preprint arXiv:1704.01155*, 2017.
- [43] Haichao Zhang and Jianyu Wang. Defense against adversarial attacks using feature scattering-based adversarial training. In *Advances in Neural Information Processing Systems*, 2019.
- [44] Hongyang Zhang, Yaodong Yu, Jiantao Jiao, Eric Xing, Laurent El Ghaoui, and Michael I Jordan. Theoretically principled trade-off between robustness and accuracy. In *ICML*, 2019.

SUPPLEMENTARY WORK

This supplementary work includes: noise and detailed training descriptions as well as further examples of adversarial examples for φ DNNs.

A. NOISE DESCRIPTION

Panda noise. Given a pixel $g = (R, G, B)$ in a RGB image I , Panda noise can be defined as follows:

$$f(g) = \begin{cases} g, & P = 1 - (\alpha + \beta) \\ (255, 255, 255), & P = \alpha \\ (0, 0, 0), & P = \beta \end{cases}$$

where α and β are probabilities that a pixel in image I will become respectively white or black.

ColorDepth noise. A RGB image represents feature information by color bit depths. For example, CIFAR-10 encodes images with 24-bit color depths. The ColorDepth noise reduces original images to fewer bits representation. Given a normalized RGB image I that ranges from 0 to 1, and the target t-bits color depths after reducing, this noise could be formulated as:

$$I' = \frac{[I \cdot (2^t - 1)]}{2^t - 1}$$

where $[\]$ denotes the standard rounding function and I' is the image encoded with t-bits color depths.

Gaussian noise. Given a RGB image I , the Gaussian noise could be described as the following:

$$I' = I + R \sim \mathcal{N}(\mu, \sigma^2)$$

where R is the Gaussian filter.

B. TRAINING STRATEGY

We use Adam with learning scheduler in all experiments. Due to the poor performance of Adam in the adversarial training, the SGD with learning scheduler is used during the adversarial training. To improve neural network performance, we use learning scheduler to adjust learning rate. For Adam learning scheduler, the learning rate starts from 10^{-3} and increases to 10^{-1} then decreases to 10^{-2} , 10^{-3} and $0.5 * 10^{-3}$. For SGD learning scheduler, the learning rate starts from 10^{-1} and decreases to 10^{-2} and 10^{-3} . To match data normalization, we apply sigmoid activation function instead of tanh as the last layer output for generator model in SRGAN.

C. EXAMPLES OF IMAGES PROCESSED BY φ DNNs

Figure 6 to 8 contain some samples and the images from each stage of the φ_r DNN when processing these samples. Figure 9 to 14 follows a similar pattern but for φ_i DNN.

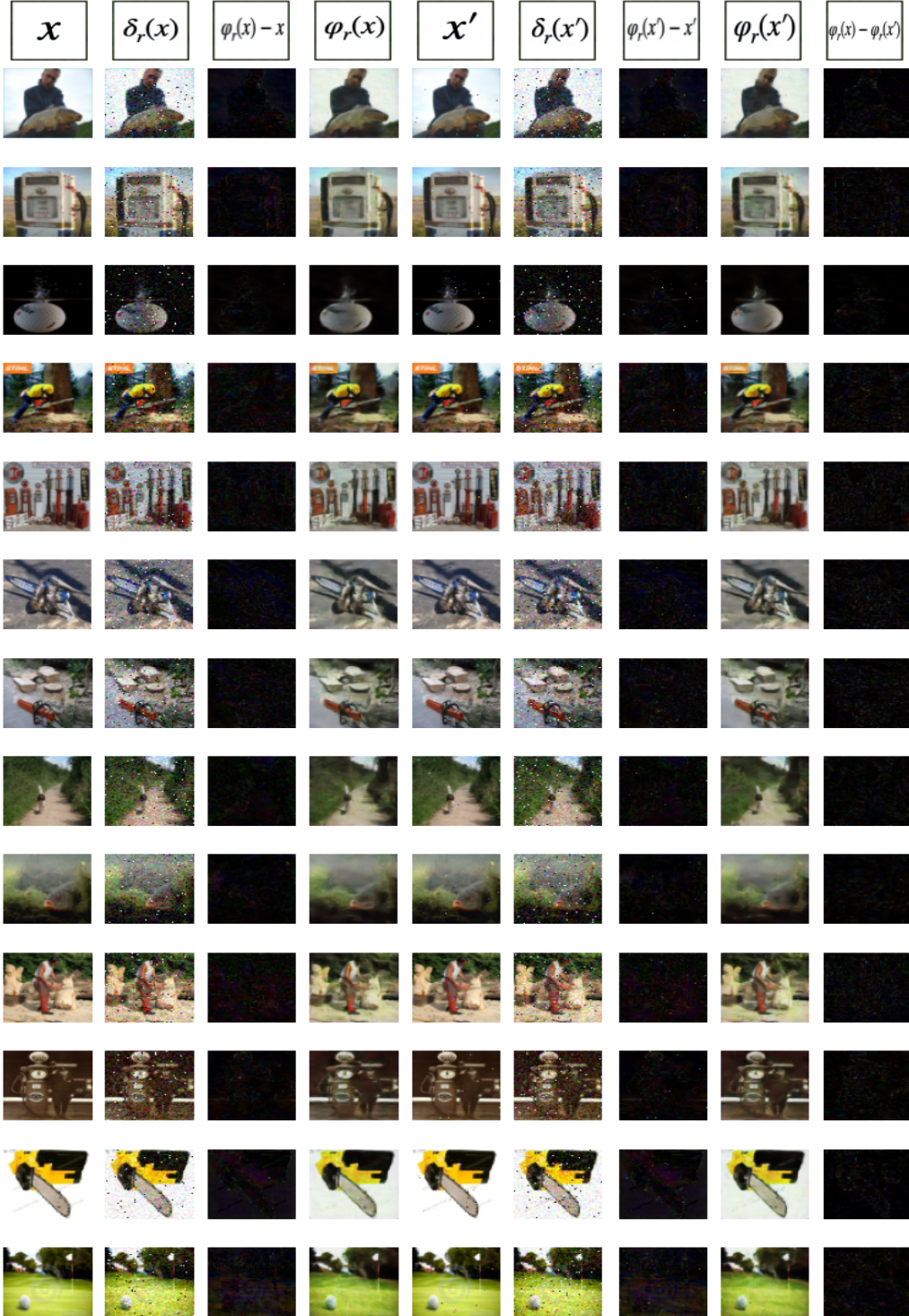


Figure 6: Examples of $\varphi_r(x)$ for an Imagenette’s image x and its respective adversarial sample x' . The adversarial samples were built with 10px attack.



Figure 7: Examples of $\varphi_r(x)$ for a CIFAR10’s image x and its respective adversarial sample x' . The adversarial samples were built with 10px attack.



Figure 8: Examples of $\varphi_r(x)$ for an CIFAR10's image x and its respective adversarial sample x' . The adversarial samples were built with 10px attack.

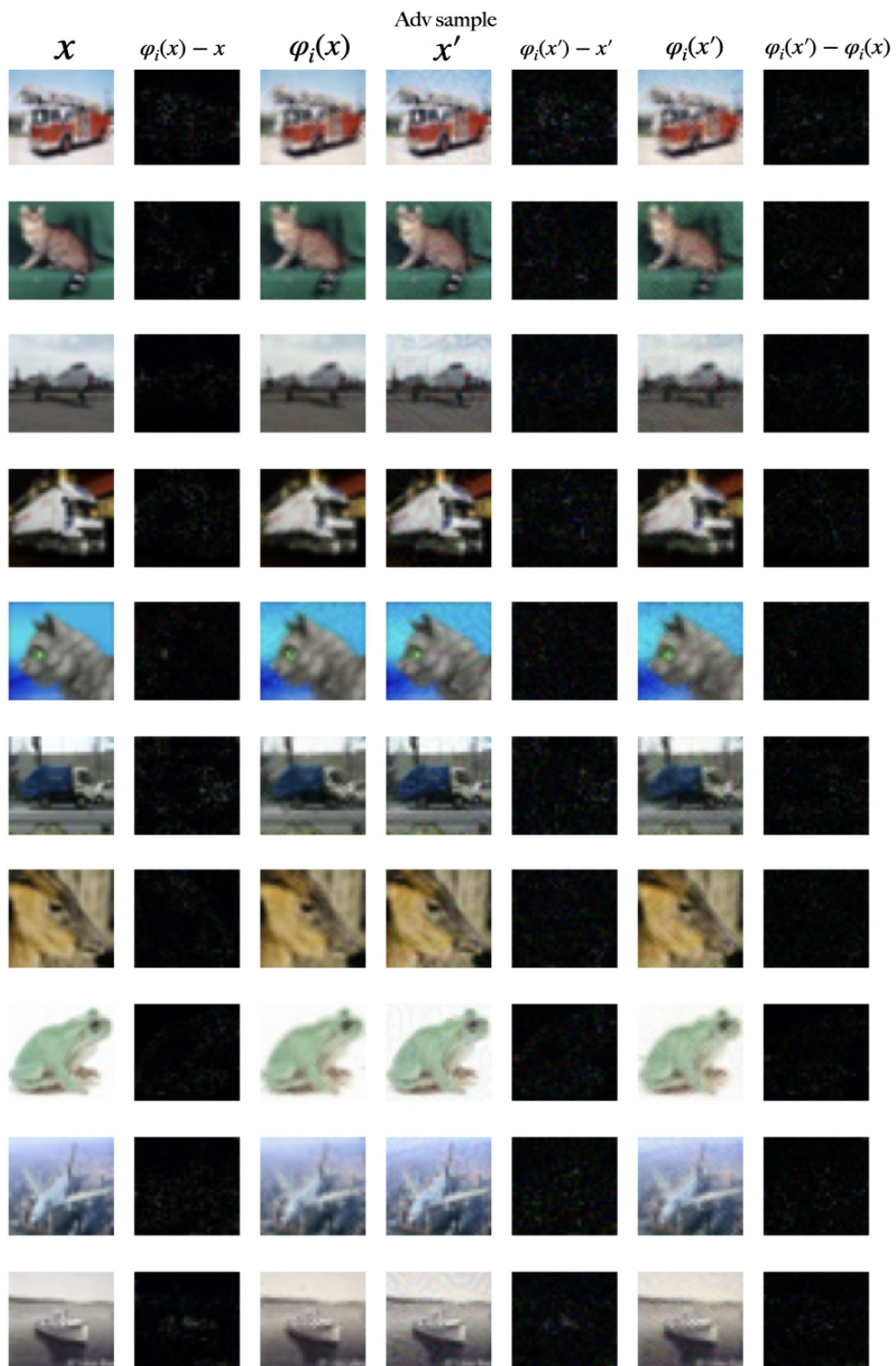


Figure 9: Examples of $\varphi_i(x)$ for an CIFAR10's image x and its respective adversarial sample x' . The adversarial samples were built with PGD.

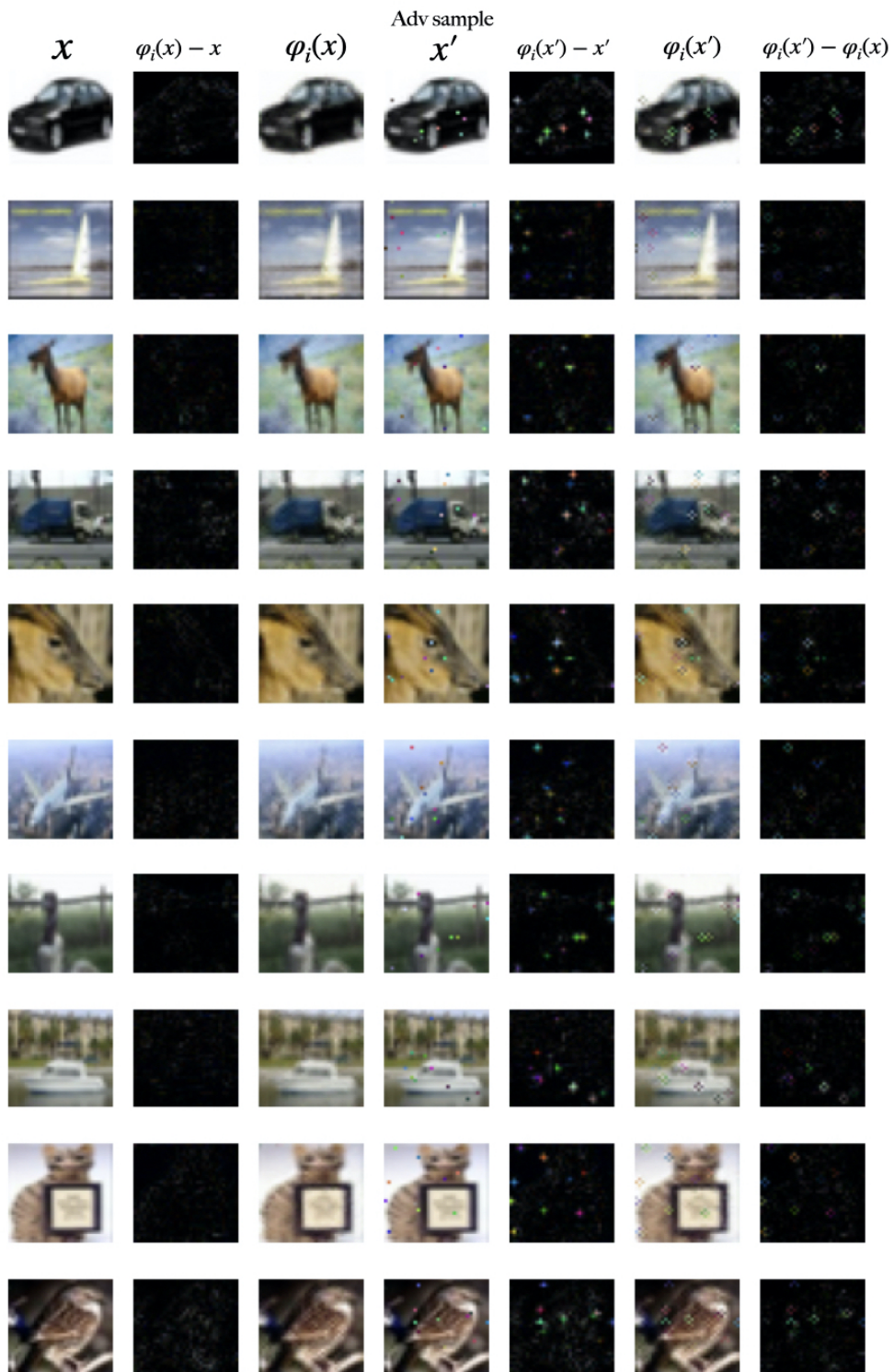


Figure 10: Examples of $\varphi_i(x)$ for a CIFAR10's image x and its respective adversarial sample x' . The adversarial samples were built with 10px attack.



Figure 11: Examples of $\varphi_i(x)$ for an SVHN's image x and its respective adversarial sample x' . The adversarial samples were built with PGD.

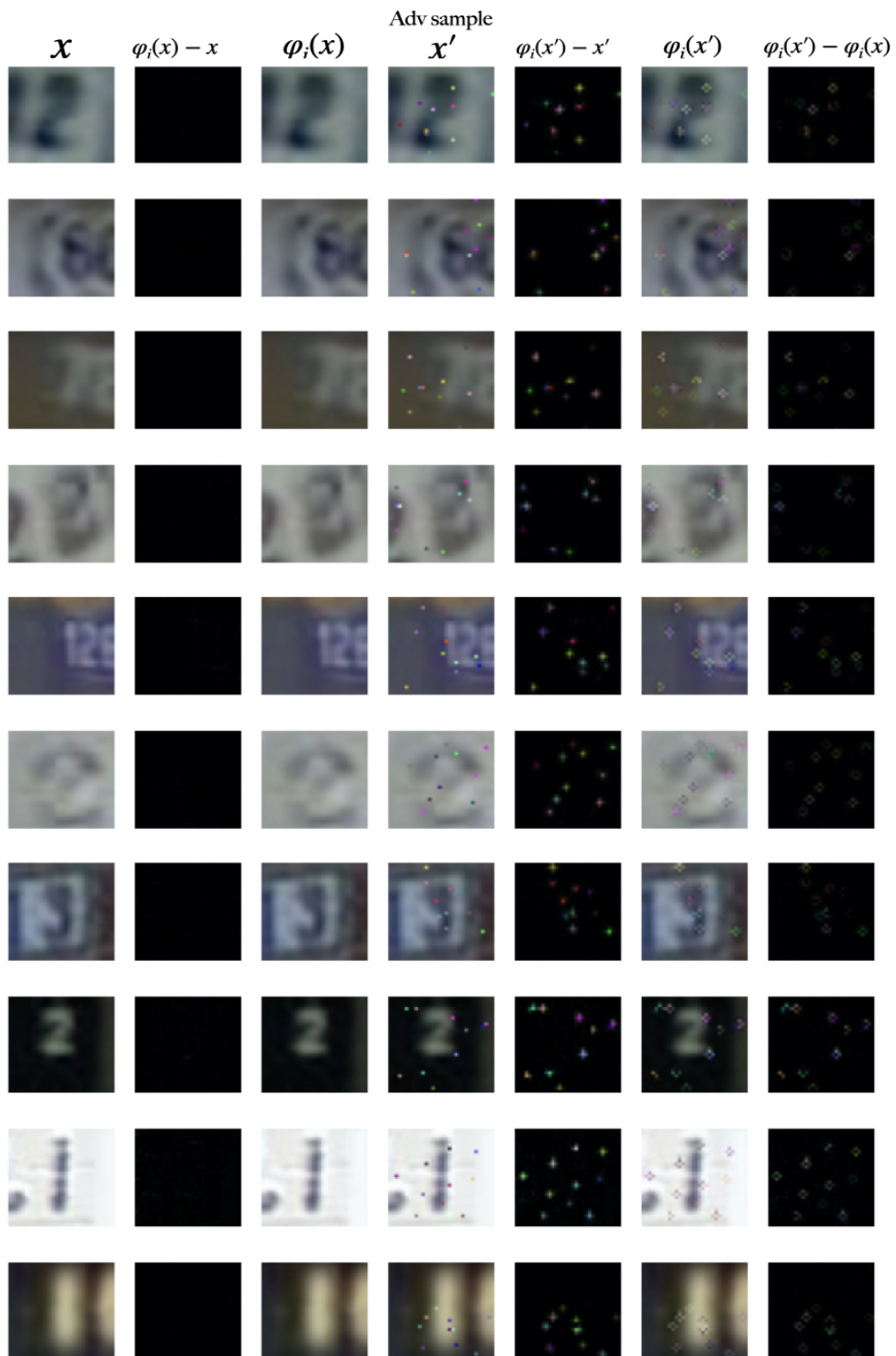


Figure 12: Examples of $\varphi_i(x)$ for an SVHN's image x and its respective adversarial sample x' . The adversarial samples were built with 10px attack.

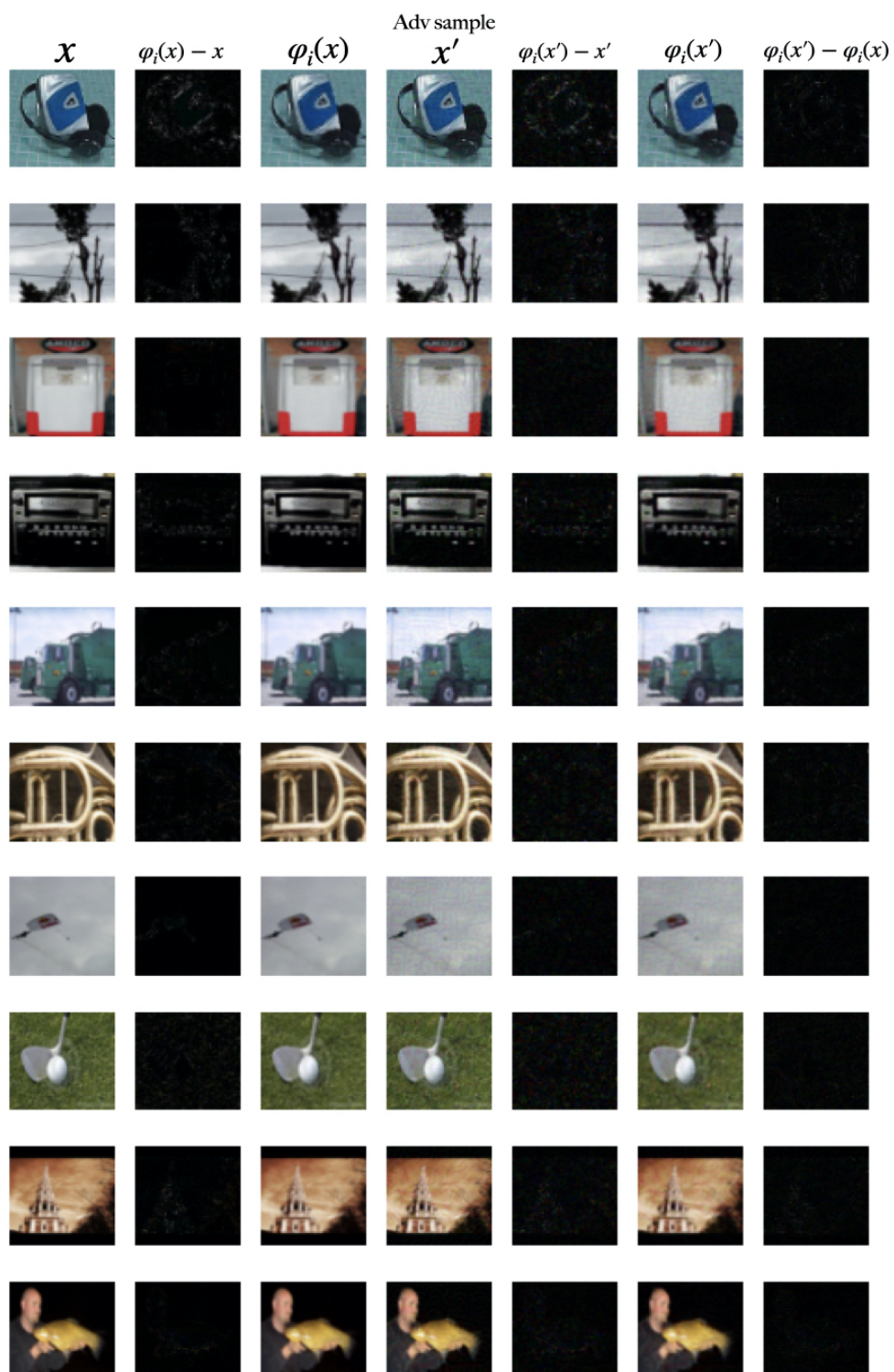


Figure 13: Examples of $\varphi_i(x)$ for an Imagenette’s image x and its respective adversarial sample x' . The adversarial samples were built with PGD.

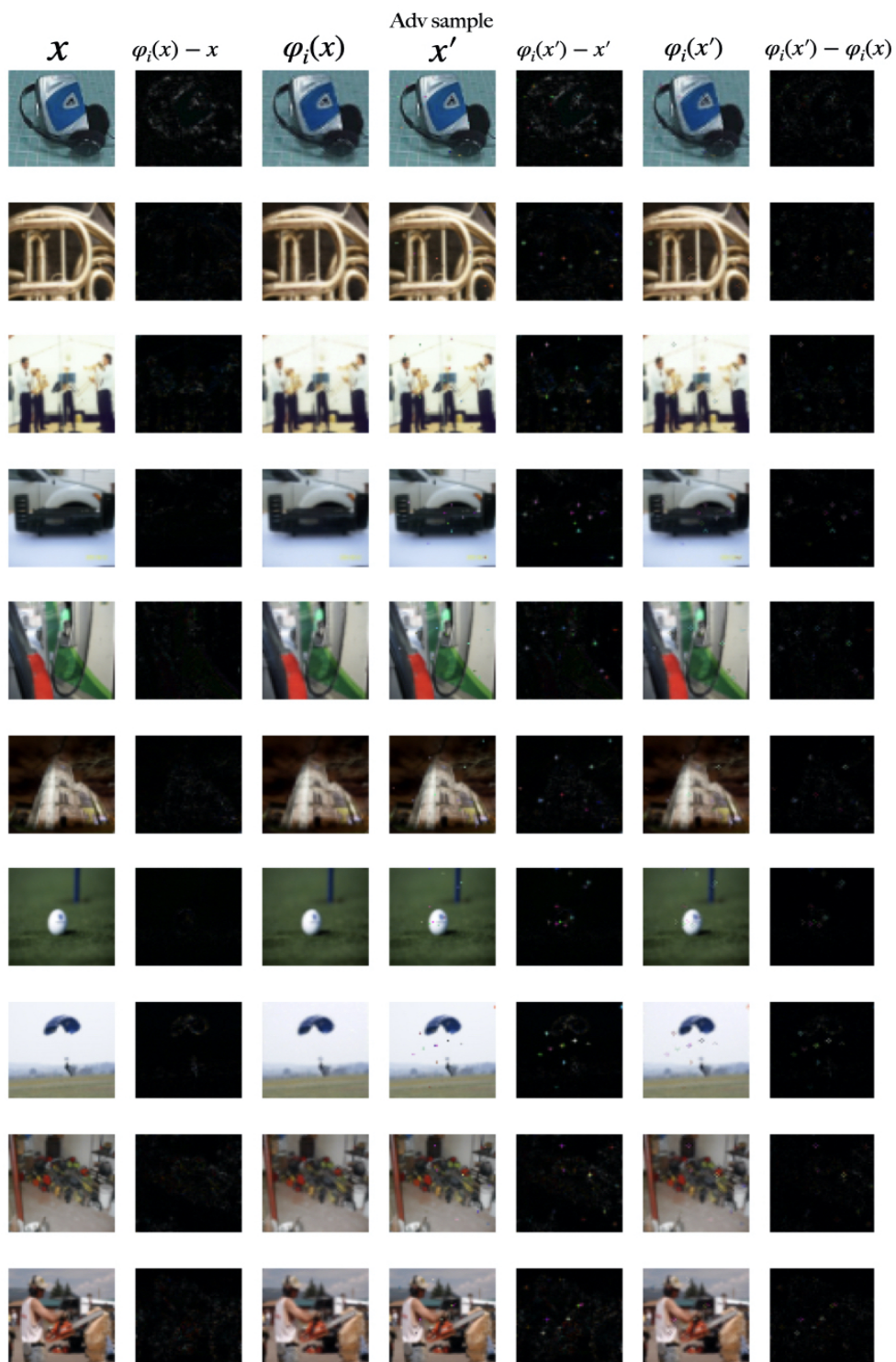


Figure 14: Examples of $\varphi_i(x)$ for an Imagenette’s image x and its respective adversarial sample x' . The adversarial samples were built with 10px attack.